Electron Pitch Angle Distributions in Compressional Pc5 Waves by THEMIS-A Observations

X. Ma[1,2], A. M. Tian[1,2†], Q. Q. Shi[1], S. C. Bai[1], S. T. Yao[1], X. C. Shen[3], W. J. Sun[4], R. L. Guo[1], M. Nowada[1], A. W. Degeling[1], J. Liu[1], L. Li[5], S. Zhang[1], W. Li[2]

[1]*Shandong Key Laboratory of Optical Astronomy and Solar-Terrestrial Environment, School of Space Science and Physics, Institute of Space Sciences, Shandong University, Weihai, Shandong 264209, People's Republic of China*

[2]*State Key Laboratory of Space Weather, Chinese Academy of Sciences, Beijing 100190*

[3]*Center for Space Physics, Boston University, Boston, MA, USA*

[4]*Department of Climate and Space Sciences and Engineering, University of Michigan, Ann Arbor, MI, USA*

[5]*School of Earth and Space Sciences, Peking University, Beijing, China*

Corresponding author: A. M. Tian (tamin@sdu.edu.cn)

Key points

- Cigar, butterfly, and pancake electron pitch angle distributions are found in the magnetic troughs of compressional Pc5 waves.
- Electron pitch angle distributions show different energy dependences in whistler- and nonwhistler-type compressional Pc5 waves.
- Electron pitch angle distribution features in compressional waves could be related to Landau resonance and drift shell splitting.

Abstract

Although compressional Pc5 waves are well known in the energy conversion and regulation of charged particles in the magnetosphere, the detailed features of associated electron pitch angle distributions (ePADs) are poorly understood. Based on Time History of Events and Macroscale Interactions during Substorms (THEMIS) observations from 2010 to 2016, ePADs in the magnetic decreases (troughs) of compressional Pc5 waves are classified into three types: cigar, butterfly, and pancake. They are found in the electrons with respective energy ranges of 100–1000 eV (larger than 10 keV), 1–10 keV (larger than 1 keV), and 6–30 keV (100 eV–10 keV) in (non)whistler-type compressional Pc5 waves, that is, cases where whistler-mode waves are present (absent) in the magnetic troughs. These statistical ePAD features observed in the whistler- and nonwhistler-

This is the author manuscript accepted for publication and has undergone full peer review but has not been through the copyediting, typesetting, pagination and proofreading process, which may lead to differences between this version and the Version of Record. Please cite this article as doi: 10.1029/2021GL095730.

type waves are suggested to be associated with the Landau resonance of whistler-mode waves and drift-shell splitting effect.

Plain language summary

Ultralow frequency (ULF) waves play a significant role in modifying the charged particles in the magnetosphere. In compressional Pc5 waves, each magnetic trough can be considered a mirror-like structure. Therefore, such waves can significantly modulate charged particles. Studying the ePADs in compressional Pc5 waves is crucial for understanding the dynamic behaviors of electrons. Using THEMIS-A data, we present a statistical study to investigate ePADs in compressional Pc5 waves. ePADs are mainly observed in three types: cigar, butterfly, and pancake. Each of the ePADs shows a different energy dependence in two types of compressional waves. The two types of events are defined based on the presence or absence of whistler-mode waves in the magnetic troughs of compressional Pc5 waves. The statistical results suggest that the ePADs in nonwhistler-type compressional waves are affected by the background ePADs. For whistler-type compressional waves, whistler wave-particle interactions might be important, suggesting a cross-scale coupling of the energy transport in compressional Pc5 waves.

1. Introduction

Ultralow frequency (ULF) waves play an important role in the acceleration and modulation of charged particles in the Earth's magnetosphere (Zong et al., 2007, 2009; Zhou et al., 2015, 2016). Compressional waves within the Pc5 range (150~600-s period) are often observed in the two flanks of the Earth's magnetosphere (Takahashi et al., 1985, 1987b; Zhu and Kivelson, 1991; Constantinescu et al., 2009; Li et al., 2017a, 2017b). In the magnetic troughs of compressional waves, charged particles often show trapping signatures, indicating that the waves are mirror-like structures (Rae et al., 2007; Liu et al., 2016; Tian et al., 2012, 2020). Their magnetic pressure and thermal pressure are usually in anti-phase, while the total pressure remains almost constant. These waves are commonly thought to be excited by internal sources, such as drift mirror instability and drift ballooning instability, which result from high β (the ratio of the thermal pressure to the magnetic pressure) and large perpendicular pressure anisotropy (Hasegawa, 1969; Cheng and Qian, 1994). Mirror-mode structures can be widely observed in space, such as in the Earth's magnetosheath, magnetotail, solar wind, and comet (Zhang et al., 2008; Nowada et al. 2009; Xiao et al., 2010, 2014; Sun et al., 2012; Yao et al., 2019b, 2020; Russell et al., 1987).

Whistler-mode waves with typical frequencies from 0.1 to 1 f_{ce} are often observed in the

Earth's magnetosphere, where f_{ce} refers to the electron gyrofrequency (Tsurutani and Smith, 1974). They are commonly observed outside the plasmapause, from the pre-midnight to the afternoon sector near the equatorial plane (e.g., Li et al., 2009, 2010). It is generally accepted that whistler-mode waves are excited by the cyclotron resonance of a few to tens of keV anisotropic electrons (Kennel and Petschek, 1966; Tsurutani and Smith, 1974; Omura et al., 2004; Yao et al., 2019a). Whistler-mode waves can strongly interact with electrons via cyclotron and Landau resonances, resulting in pitch angle scattering (Kennel and Petschek, 1966; Horne et al., 2003; Thorne et al., 2010). They have been frequently observed in the magnetic troughs of compressional Pc5 waves and the mirror-mode structures in the magnetosheath, where the electron temperature anisotropy is high (e.g., Thorne and Tsurutani, 1981; Li et al., 2011; Xia et al., 2016; Zhang et al., 2019; Kitamura et al., 2020).

Numerous studies have suggested that mirror-mode structures can significantly modulate charged particles, resulting in various PADs (Southwood and Kivelson, 1993; Chisham et al., 1998; Soucek et al., 2011; Yao et al., 2017, 2018). However, the modulations of electrons by compressional Pc5 waves in the magnetosphere have not been systematically studied. In particular, the environments in the magnetosphere are different from those in the magnetosheath and solar wind. For instance, the two ends of the magnetic field lines in the magnetosphere are connected to the ionosphere, and the magnetic field strength and the thermal pressure generally have radial gradients in the equatorial plane. In such a plasma environment, the background ePADs are basically different from those of the solar wind and magnetosheath. In this study, based on the 2010-2016 data from THEMIS-A, we focus on the ePADs in compressional Pc5 waves and investigate the formations of the different ePADs.

2. Data and method

The THEMIS spacecraft was launched in 2007 and is composed of five identical probes in near-equatorial orbits (Angelopoulos, 2008). The apogees and perigees of THEMIS A, D, and E are above 10 R_E (1 R_E refers to one Earth's radius) and below 2 R_E. The fluxgate magnetometer (FGM) provides 3-s resolution spin-averaged magnetic field data (Auster et al., 2008). The electrostatic analyzer (ESA) measures 3-D distributions of ions and electrons ranging from a few eV to 30 keV with 3-s resolution (McFadden et al., 2008). The search coil magnetometer (SCM; Roux et al., 2008; Le Contel et al., 2008) measures magnetic fields from 0.1 Hz to 4 kHz. The digital field board (DFB; Cully et al., 2008) can process the waveforms provided by the SCM, and

the survey mode data cover most of the orbits from 2 Hz to 4 kHz, which can be used to identify whistler-mode waves. With these equipped instruments, the THEMIS spacecraft provides us with an excellent opportunity to investigate the ePADs in compressional Pc5 waves.

The classification of the ePAD types at the magnetic field troughs of compressional waves is similar to that in previous studies (Ni et al., 2016; Liu et al., 2020; Li et al., 2020). Two indices are defined for PAD identification: γ = G/F and BI = F/C, where G, F, and C are the averaged electron flux at pitch angles $\in$ [0°, 25°] & [155°, 180°], [25°, 75°] & [105°, 155°], and [75°, 105°], respectively. Consequently, the ePADs in the magnetic troughs can be classified into three types: cigar (with maximum flux at small pitch angles, i.e., BI > 0.95 and γ > 1.05), butterfly (with maximum flux at intermediate pitch angles, i.e., BI > 1.00 and γ < 0.95), and pancake (with maximum flux at large pitch angles, i.e., BI < 0.95 and γ < 0.95). Typical examples of the ePADs are shown in Figure 1.

Because of the possible interactions between the whistler-mode waves and the electrons, we divide the compressional Pc5 waves into two groups: whistler- (whistler-mode waves are observed in the magnetic troughs) and nonwhistler-types (whistler-mode waves are absent). Since the identified whistler-type events in this study show that the frequency of whistler emissions can barely extend to above 0.5 f_{ce}, the integrated magnitude over 0.05–0.5 f_{ce} for the whistler-mode wave has been used to characterize the wave intensity (e.g., Li et al., 2011). We take 10 pT as the threshold to determine the presence of whistler-mode waves.

3. Observations

Figure 1 shows two types of compressional Pc5 waves with whistler-mode waves (left column) and without whistler-mode waves (nonwhistler, right column). For both cases, the magnetic compressional components (B_z) dominate the fluctuations and oscillate with periods of ~10 mins and ~2.5 mins, respectively (Figure 1 (a1, a2) and (b1, b2)). Figure 1 (c1, c2) shows the electron number density N_e inferred from the spacecraft potential (Li et al., 2010). The electron density oscillates in anti-phase with B_t in case 1 but oscillates in-phase with B_t in case 2. For both cases, the ion perpendicular temperatures are higher than the parallel temperatures and vary in anti-phase with B_t, while the electron temperatures are different (Figure 1 (d1, d2) and (e1, e2)). For case 1, the electron perpendicular temperature $T_{e\perp}$ is larger than the parallel temperature $T_{e//}$ most of the time, which is the opposite of case 2. In addition, the electron temperatures generally vary in anti-phase with B_t in case 1 but in-phase with B_t in case 2. Figure 1 (f1, f2) shows the plasma thermal

pressure (red, calculated by $n_i k_b T_{i\perp} + n_e k_b T_{e\perp}$, where n_i (n_e) is the ion (electron) density, $T_{i\perp}$ ($T_{e\perp}$) is the ion (electron) perpendicular temperature and k_b is the Boltzmann constant), magnetic pressure (blue) and total pressure (black). The plasma thermal pressure and magnetic pressure are out of phase, and the total pressure maintains quasi-equilibrium. These features are consistent with those of the compressional wave events studied by Zhu and Kivelson (1994) and Korotova et al. (2009) and should be driven by drift mirror instability (Hasegawa, 1969). Interestingly, both cases exhibit "frequency-doubling" phenomenon (Takahashi et al., 1987a, 1987b, 1990; Korotova et al. 2013). Although this phenomenon is beyond the scope of this study, the related particle signatures are worth making a further study.

The behavior of electrons depends on energy and event types (Figure 1 (g1, g2)–(j1, j2)). In case 1, 10–84 eV electrons are in field-aligned directions (cigar PADs), and the flux oscillates in phase with B_t, which can be explained by the decrease in parallel velocity and accumulation of electrons at the mirror point (e.g., magnetic peak) due to conservation of the first adiabatic invariant (e.g., Kivelson and Southwood, 1996). However, for the 84–753 eV and 753 eV–6.8 keV electrons, although the ePADs are cigar type in some magnetic troughs, the flux oscillates out of phase with the magnetic field strength (Figure 1 h1–i1). Electrons at 753 eV–6.8 keV and 6.8–32 keV exhibit trapping signatures in some magnetic troughs of case 1 (Figure 1 i1–j1). These ePADs are pancake type or show the "donut" profile (butterfly ePADs in the magnetic trough centers and pancake type at the magnetic peaks). For case 2, the cold electrons (10–84 eV) are in the field-aligned directions (Figure 1 g2), while for 84–753 eV electrons, the PADs are pancake type (Figure 1 h2). However, in contrast to case 1, the electrons at 753 eV–6.8 keV and 6.8–32 keV show cigar and butterfly PADs in most of the magnetic troughs (Figure 1 i2, j2). Figure 1 (m1–p1) and (m2–p2) show the details of Figure 1 (a1, h1–j1) and (a2, h2–j2) for two magnetic troughs of whistler-type and nonwhistler-type, respectively. Because we mainly focus on the ePADs in magnetic troughs, the donut-shaped ePADs will be identified as the butterfly type in the following text.

In case 1, the whistler-mode waves are localized in the magnetic troughs (Figure 1 (k1, k2)), suggesting that the local magnetic minimum with high electron density could be the source region of the whistler-mode waves (Li et al., 2011; Ahmadi et al., 2018; Kitamura et al., 2020). Interestingly, the unusual field-aligned (Figure 1 hi–i1) and butterfly (Figure 1 i1–j1) electrons in the magnetic troughs in case 1 coexist with the whistler-mode waves, which will be discussed in section 5. In case 2, whistler-mode waves are absent throughout the event.

4. Statistical results

Figure 2 represents the statistical results of the ePADs of the whistler- (Figure 2a–2e) and nonwhistler-type (Figure 2f–2j) compressional waves from 2010 to 2016 observed by THEMIS-A. The compressional Pc5 wave events are visually selected based on the following criteria: 1. the magnetic fluctuation is dominated by the compressional component and in the Pc5 frequency band; 2. the 3-s resolution ePAD data are available to identify the types of ePADs; and 3. the DFB data are available to identify the whistler-mode waves. The compressional waves that lasted more than 1 hour are divided into several events in units of 1 hour. We obtain 1,167 events in total, including 670 whistler-type and 497 nonwhistler-type events.

Figures 2a and 2f show the spatial distributions of whistler- and nonwhistler-types of compressional Pc5 wave events in the X–Y plane in GSM coordinates, respectively. The orbit distributions of THEMIS-A are nearly uniform from 2010 to 2016; hence, the distribution of the number of events can represent the distribution of the incidence of events. Both types of waves show dawn-dusk asymmetry. In Figure 2a, the number of whistler-type events on the dawnside (64%, 431 events) is greater than that on the duskside (36%, 239 events). The possible reason for this phenomenon is that whistler-mode waves are more easily excited in the dawnside magnetosphere (e.g., Li et al., 2010). In contrast, nonwhistler-type events are less frequently observed on the dawnside (4%, 21 events), and 476 wave events (96%) are observed on the duskside.

Figure 2 (b)–(d) and (g)–(i) show the statistics of the ePADs in the magnetic troughs. Magnetic field variation $\Delta B/B$ in the troughs should be larger than 0.15. The total samples of the whistler and nonwhistler magnetic troughs are 4,257 and 5,407, respectively. Each sample is a local magnetic minimum (3-s measurement) in the magnetic trough. The histogram represents the proportion of each PAD type in each energy bin. For both types of magnetic troughs, more than 70% of the ePADs are the cigar type in the energy range of 10–80 eV. These cold populations may originate from the ionosphere. For whistler-type magnetic troughs, ePADs exhibit a clear energy dependence (Figure 2b–2d). The occurrence rates of the cigar, butterfly, and pancake ePADs are 82%, 69%, and 65% at energy ranges from 100 eV–1 keV, 1–10 keV, and 3–30 keV, respectively. However, the occurrence rates of the cigar, butterfly, and pancake ePADs in nonwhistler-type magnetic troughs are 31%, 71%, and 90% at energy ranges from >10 keV, >1 keV, and 100 eV–10 keV, respectively. In nonwhistler-type magnetic troughs, cigar ePADs show a higher

occurrence rate of >10 keV electrons than 100 eV–10 keV electrons. The butterfly PADs of >1 keV electrons exhibit a slightly higher occurrence rate than 10 eV–1 keV electrons. The pancake ePADs show ~50% occurrence for 100 eV–10 keV electrons and a lower occurrence rate of >10 keV electrons compared with 100 eV–10 keV electrons. Since B and Je (the flux of electrons with cigar PAD) in magnetic troughs exhibit in-phase or anti-phase oscillations, we classify cigar PAD into either in-phase or anti-phase B-Je type. For 10–84 eV electrons in whistler-type magnetic troughs, the occurrence rate of cigar ePADs with anti-phase B-Je is less than 50% (Figure 2e). A similar feature can be seen in a broad energy range (10 eV–20 keV) in nonwhistler-type magnetic troughs (Figure 2j). However, for several hundreds of eV electrons with cigar PADs in whistler-type magnetic troughs, most of them (~75%) exhibit anti-phase B-Je.

5. Discussion

The ePADs in compressional waves show features that differ from those of mirror-mode waves in magnetosheath or solar winds (e.g., Chisham et al., 1998; Yao et al., 2018; Wang et al., 2020). To understand the formation of different types of ePADs in these events, the following two aspects must be considered: whistler wave-particle interactions and the background ePADs.

5.1 Whistler Wave-Particle Interactions

Figure 3a shows the electron pitch angle-energy spectrogram at the magnetic minimum (2015-10-28/18:48:58, UT) of a whistler-type magnetic trough in case 1. To show anisotropy more clearly, electron phase space densities (PSDs) in each energy bin are normalized by the averaged PSDs in the energy bin (e.g., Kitamura et al., 2020). The findings suggest that the perpendicular energies of the electrons with the maximum PSD increase gradually with increasing energy from 100 eV to 1 keV, i.e., with increasing energy, the ePADs successively present cigar, butterfly and pancake types. To verify the roles of the whistler waves in the ePADs, the Landau (solid curves) and cyclotron (dashed curves) resonant energy (E_R=E*cos^2(PA), where E_R is resonant energy, E is electron total energy and PA is the electron pitch angle) curves are overlapped in Figure 3a. Landau and cyclotron resonant energies are calculated based on the following formula (Lengyel-Frey et al., 1994): $E_R = \frac{B_0^2}{2\mu_0 N_e} \frac{\Omega}{\omega\, cos^2\theta} \left(cos\theta - \frac{\omega}{\Omega}\right)\left(m + \frac{\omega}{\Omega}\right)^2$, where E_R is the resonant energy, B_0 is the background magnetic field, N_e is the electron number density, θ is the wave normal angle (WNA, which is assumed to be 0° since the WNA data are absent from the DFB), ω is the frequency of the whistler-mode waves (identified as the frequency with the maximum wave power in the

magnetic field spectrogram), Ω is the electron gyrofrequency, and m = 0 and -1 correspond to the Landau and cyclotron resonances, respectively. Figure 3a suggests that the Landau resonant energy curves have a similar trend with the peaks of the electron PSDs in the energy range from 100 eV–1 keV. This result indicates that cigar and butterfly ePADs are probably produced via Landau resonance (e.g., Min et al., 2014). The crosses in Figure 3a represent the points to calculate parallel energies $E_{\mathrm{fmax}}*\cos^2(PA_{\mathrm{fmax}})$ in different pitch angle bins, where E_{fmax} and PA_{fmax} are the energies and pitch angles of the peaks of the electron PSDs. The averaged value of the parallel energies E_{Robs} represents the expected Landau resonant energy of these magnetic troughs. We confine the pitch angle bins to 0°–60° and 120°–180° because the Landau resonance is more effective in changing the PSDs of electrons with small pitch angles (e.g., Min et al., 2014). The calculated E_{Robs} is 173.86 eV, which is close to the Landau resonant energy of 139 eV, as calculated with B_0=22.3 nT, N_e=1.08 cm^{-3}, ω=132 Hz, and Ω=624 Hz. Moreover, the minimum cyclotron resonant energy is 1938 eV, which is lower than the energies (> 4 keV) of the trapped anisotropic electrons, suggesting that whistler-mode waves may be excited by electrons with pancake PADs (e.g., Li et al., 2011).

Figure 3b shows the correlation of two resonant energies (hot and cool colored dots denote Landau and cyclotron resonance, respectively) with E_{Robs} for all 4257 whistler-type magnetic troughs. The vertical error bars in Figure 3b represent one standard deviation of the parallel energies. The horizontal error bars in Figure 3b represent the errors of Landau resonant energy from the uncertainties of the WNA (assuming that the maximum θ is 45° since the WNA data are absent from the DFB). Two colored bars in Figure 3b represent the ratios between the whistler-mode wave frequency and the electron gyrofrequency. With increasing Landau (cyclotron) resonant energies, the whistler-mode wave frequency tends to increase (decrease), which is consistent with the formula of the resonant energies. The correlation coefficient of the Landau resonant energies and E_{Robs} is 0.79, indicating that the peaks of the electron PSDs may be caused by the Landau resonance. Furthermore, most of the cyclotron energies (cool color dots) are in the energy range of a few to tens of keV, which is consistent with the energy range (3–30 keV) of the majority of the pancake ePADs (Figure 2d). This finding suggests that whistler-mode waves are probably generated by the electrons of pancake PADs via cyclotron resonance. The generated whistler-mode waves can accelerate hundreds of eV electrons via Landau resonance; hence, strong field-aligned electrons (cigar PADs) and butterfly PADs are formed.

Previous observations and simulations of the electrons in mirror-mode structures suggest that the electrons often exhibit butterfly or "donut-shaped" PADs (Chisham et al., 1998; Yao et al., 2018; Li et al., 2021). The authors explained that these PAD features were primarily caused by the betatron cooling effect and the Fermi acceleration during the deepening of the magnetic troughs. However, this phenomenon cannot explain the energy dependence of the ePADs in some observations (e.g., Ahmadi et al., 2018; Breuillard et al., 2018; Kitamura et al., 2020) and the pancake ePADs of a few to tens of keV in our observations. Furthermore, according to the formula of the perturbation of the plasma PSD: $\delta f = \mu b_{\parallel}(1/T_{\perp}-1/T_{\parallel})f$, where μ is the first adiabatic invariant, $b_{\parallel}$ is the compressional component of the magnetic field, $T_{\perp}$ and $T_{\parallel}$ are plasma perpendicular and parallel temperatures and f is the plasma PSD (Zhu and Kivelson, 1994). In the two circumstances, i.e., when the background ePADs are cigar type ($T_{\parallel}>T_{\perp}$), the PSDs will be in phase with $b_{\parallel}$ (Figure 1(g1), Figure (2e, 2j)). For the pancake ePADs ($T_{\parallel}<T_{\perp}$), the PSDs will be in anti-phase with $b_{\parallel}$ (Figure 1(j1, h2)). These features of particle modulations were also confirmed in prior observations (e.g., Tian et al., 2020). However, the above theories cannot explain why, during whistler-type events, anti-phase B-Je oscillations occur more often than in-phase B-Je oscillations at energies (100–1000 eV) dominated by cigar-type electron PAD (Figure 1(h1, i1), Figure 2e). Our analyses explain that the energy dependence of ePADs in whistler-type compressional waves is primarily caused by whistler wave-particle interactions.

5.2 Electron Drift Shell Splitting Effect

Figure 3c shows the electron pitch angle-energy spectrogram at a magnetic minimum (07:41:30 UT) in case 2. At this magnetic minimum, 100 eV–1 keV electrons show pancake PADs, while 1–2 keV and 2–32 keV electrons exhibit butterfly and cigar PADs, respectively. The statistical results (Figure 2g–2i) suggest that for >10 keV electrons, the cigar and pancake ePADs show a higher and lower occurrence rate of >10 keV electrons compared with 100 eV–10 keV electrons, respectively. In addition, the butterfly PADs of >1 keV electrons show a higher occurrence rate than 10 eV–1 keV electrons. Since nonwhistler-type compressional waves tend to occur on the duskside (96%), the drift shell splitting effect (Roederer 1967; Sibeck et al., 1987) is considered to be a possible scenario. On the dayside magnetosphere with the large L (L>7), the electron flux usually has a negative gradient with L (e.g., West et al., 1973), and the electrons often show pancake PADs (e.g., Li et al., 2020). Due to the drift shell splitting effect, the electrons with larger pitch angles on the duskside are from the noonside with higher L-shells, as shown in the

diagram (Figure 3d). Consequently, the flux of electrons with a larger pitch angle on the duskside will be lower than that of electrons with a smaller pitch angle. Hence, the electrons on the duskside will exhibit cigar or butterfly PADs when the gradient of the electron flux on the noonside is steeper. As a result, the electrons in the duskside magnetosphere do not have enough perpendicular anisotropy to excite whistler-mode waves. In particular, Figure 1 (i2, j2) suggests that the "donut-shaped" ePADs in the nonwhistler-type events are formed by modulations of the compressional Pc5 waves to the electrons with butterfly background PADs. This scenario is obviously different from the formation of the "donut-shaped" ePADs in whistler-type compressional waves, which may be dominated by the Landau resonance of whistler-mode waves. Moreover, the increasing (decreasing) occurrence rate of cigar (pancake) ePADs in the energy range of >10 keV supports the idea of drift-shell splitting because the negative gradients of electron flux become steeper with increasing electron energy (e.g., West et al., 1973). These features suggest that without the interactions of whistler-mode waves, the drift shell splitting effect dominates the formation of energy dependent ePADs in nonwhistler-type compressional waves.

6. Summary

In this study, we investigate the ePADs in compressional Pc5 waves from 2010 to 2016 by THEMIS-A observations. The results are summarized as follows:

1. ePADs are significantly different in compressional Pc5 waves with and without whistler-mode waves inside the magnetic troughs. Cigar, butterfly, and pancake ePADs in the two types of compressional Pc5 waves exhibit different energy dependences. In whistler-type compressional waves, cigar, butterfly, and pancake ePADs tend to occur in the energy ranges from 100–1000 eV, 1–10 keV, and 6–30 keV, respectively. In nonwhistler-type compressional waves, the occurrence rates of cigar and pancake PADs for electrons with energy larger than 10 keV are higher and lower than those of 100 eV–10 keV electrons, respectively. The butterfly ePADs show a higher occurrence rate in the energy range >1 keV than that in 10 eV–1 keV.
2. In whistler-type compressional Pc5 waves, whistler wave-particle interactions are important. Whistler-mode waves inside the magnetic troughs of compressional waves may be generated locally by the electrons with pancake PADs via cyclotron resonance. These whistler-mode waves can greatly accelerate electrons with energies of hundreds of eV via Landau resonance; hence, cigar and butterfly ePADs are formed. The unique features of

ePADs in whistler-type compressional Pc5 waves reveal a "cascading"-type energy transport process from compressional Pc5 waves (large scale) to whistler-mode waves and electrons (small scale).

3. In nonwhistler-type compressional Pc5 waves, drift shell splitting effect is a possible formation mechanism of energy dependent ePADs and the significant dawn-dusk asymmetry of occurrence rate of compressional Pc5 waves.

Acknowledgments. This work was supported by the Shandong University (Weihai) Future Plan for Young Scholars (2017WHWLJH08), the Specialized Research Fund for State key laboratories, National Natural Science Foundation of China (Grants 41774153, 41774172, 41974189, 41941001, 4207040247, and 41961130382) and the Royal Society NAF\R1\191047. We acknowledge V. Angelopoulos for the use of data from the THEMIS Mission; A. Roux and O. Le Contel for the use of SCM data; C. W. Carlson and J. P. McFadden for the use of ESA data; D. Larson; and K. H. Glassmeier, U. Auster, and W. Baumjohann for the use of FGM data. All the data for this paper are available at the THEMIS data depository: http://themis.ssl.berkeley.edu/data/themis/. Data access and processing was done using the Space Physics Environment Data Analysis System (SPEDAS) V3.2 (see Angelopoulos et al., 2019).

References

Ahmadi, N., Wilder, F. D., Ergun, R. E., Argall, M., Usanova, M. E., Breuillard, H., et al. (2018). Generation of electron whistler waves at the mirror mode magnetic holes: MMS observations and PIC simulation. Journal of Geophysical Research: Space Physics, 123, 6383–6393. https://doi.org/10.1029/2018JA025452

Angelopoulos. V., (2008), The THEMIS mission, Space Sci. Rev., 141, 5-34, doi:10.1007/s11214-008-9336-1.

Angelopoulos, V., Cruce, P., Drozdov, A., Grimes, E.W., Hatzigeorgiu, N., King, D. A., & Schroeder, P. (2019). The Space Physics Environment Data Analysis System (SPEDAS). Space Science Reviews, 215, 9. https://doi.org/10.1007/s11214-018-0576-4

Auster, H. U., et al. (2008), The THEMIS fluxgate magnetometer, Space Sci. Rev., 141, 235-264, doi:10.1007/s11214-008-9365-9.

Breuillard, H., Le Contel, O., Chust, T., Berthomier, M., Retino, A., Turner, D. L., et al. (2018). The properties of lion roars and electron dynamics in mirror- mode waves observed by the Magnetospheric Multiscale mission. Journal of Geophysical Research: Space Physics, 123, 93–103. https://doi.org/10.1002/2017JA024551

Chisham, G., Burgess, D., Schwartz, S. J., & Dunlop, M. W. (1998). Observations of electron distributions in magnetosheath mirror mode waves. Journal of Geophysical Research, 103(A11), 26,765–26,774. https://doi.org/10.1029/98JA02620

Cully, C. M., R. E. Ergun, K. Stevens, A. Nammari, and J. Westfall (2008), The THEMIS digital fields board, Space Sci. Rev., 141, 343-355, doi:10.1007/s11214-008-9417-1.

Cheng C Z, Qian Q (1994). Theory of ballooning-mirror instabilities for anisotropic pressure plasmas in the magnetosphere. J Geophys Res, 99: 11193–11209

Constantinescu O D, Glassmeier K H, Plaschke F, et al. (2009), THEMIS observations of duskside compressional Pc5 waves. J Geophys Res, 114: A00C25

Hasegawa A. (1969) Drift mirror instability in the magnetosphere. Phys Fluids, 12: 2642–2650

Horne, R. B., and R. M. Thorne (2003), Relativistic electron acceleration and precipitation during resonant interactions with whistler- mode chorus, Geophys. Res. Lett., 30(10), 1527, doi:10.1029/2003GL016973.

Kennel, C. F., and H. E. Petschek (1966), Limit on stably trapped particle fluxes, J. Geophys. Res., 71(1), 1.

Kitamura, N., Omura, Y., Nakamura, S., Amano, T., Boardsen, S. A., Ahmadi, N., et al. (2020). Observations of the source region of whistler mode waves in magnetosheath mirror structures. Journal of Geophysical Research: Space Physics, 125, e2019JA027488. https://doi.org/10.1029/2019JA027488

Kivelson, M. G., & Southwood, D. J. (1996). Mirror instability II: The mechanism of nonlinear saturation. Journal of Geophysical Research, 101(A8), 17,365–17,371. https://doi.org/10.1029/96JA01407

Korotova, G. I., D. G. Sibeck, V. Kondratovich, V. Angelopoulos, and O. D. Constantinescu (2009), Themis observations of compressional pulsations in the dawn-side magnetosphere, a case study, Ann. Geophys., 27, 1–11.

Korotova, G. I., D.G. Sibeck, V.Angelopoulos, and B.M.Walsh (2013), THEMIS observations of compressional poloidal pulsations in the dawnside magnetosphere: A case study, J. Geophys. Res. Space Physics, 118, 7665–7673, doi:10.1002/2013JA019360.

Kremser, G., A. Korth, J. Fejer, B. Wilken, A. Gurevich, and E. Amata (1981), Observations of quasi-periodic flux variations of energetic ions and electrons associated with Pc5 geomagnetic pulsations, J. Geophys. Res., 86(A5), 3345–3356.

Le Contel, O., et al. (2008), First results of the THEMIS searchcoil magentometers, Space Sci. Rev., 141, 509-534, doi:10.1007/s11214-008-9371-y.

Lengyel-Frey, D., Farrell, W. M., Stone, R. G., Balogh, A., & Forsyth, R. (1994). An analysis of whistler waves at interplanetary shocks. Journal of Geophysical Research, 99(A7), 13,325-13,334. https://doi.org/10.1029/94JA00781

Li, J.-H., Zhou, X.-Z., Zong, Q.-G., Yang, F., Fu, S., Yao, S., et al. (2021). On the origin of donut-shaped electron distributions within magnetic cavities. Geophysical Research Letters, 48, e2020GL091613. https://doi.org/10.1029/2020GL091613

Li, H., Peng, Q., Tang, R., Zhang, H., Zhong, Z., Deng, X., &Wang, D. (2020). Statistical characteristics of electron pitch angle distributions inside the magnetopause based on MMS observations. Journal of Geophysical Research: Space Physics, 125, e2020JA028291. https://doi.org/10.1029/2020JA028291

Li, L., Zhou, X., Zong, Q., Chen, X., Zou, H., Ren, J., & Zhang, X. (2017a). Ultralow frequency wave characteristics extracted from particle data: Application of IGSO observations. Science China Technological Sciences, 60, 419–424. https://doi.org/10.1007/s11431-016-0702-4

Li, L., Zhou, X., Zong, Q., Rankin, R., Zou, H., Liu, Y., & Hao, Y. (2017b). Charged particle behavior in localized ultralow frequency waves: Theory and observations. Geophysical Research Letters, 44, 5900–5908. https://doi.org/10.1002/2017GL073392

Li, W., et al. (2009), Evaluation of whistler-mode chorus intensification on the nightside during an injection event observed on the THEMIS spacecraft, J. Geophys. Res., 114, A00C14, doi:10.1029/2008JA013554.

Li, W., et al. (2010), THEMIS analysis of observed equatorial electron distributions responsible for the chorus excitation, J. Geophys. Res., 15, A00F11, doi:10.1029/2009JA014845.

Li, W., Thorne, R. M., Bortnik, J., Nishimura, Y., & Angelopoulos, V. (2011). Modulation of whistler mode chorus waves: 1. Role of compressional Pc4–5 pulsations. Journal of Geophysical Research, 116, A06205. https://doi.org/10.1029/2010JA016312

Liu, C. M., Fu, H. S., Liu, Y. Y., Wang, Z., Chen, G., Xu, Y., & Chen, Z. Z. (2020). Electron pitch-angle distribution in Earth's magnetotail: Pancake, cigar, isotropy, butterfly, and rolling-pin. Journal of Geophysical Research: Space Physics, 125, e2020JA027777. https://doi.org/10.1029/2020JA027777

Liu, H., et al. (2016), Compressional ULF wave modulation of energetic particles in the inner magnetosphere, J. Geophys. Res. Space Physics, 121, 6262–6276, doi:10.1002/2016JA022706.

McFadden, J. P., C. W. Carlson, D. Larson, V. Angelopoulos, M. Ludlam, R. Abiad, B. Elliott, P. Turin, and M. Marckwordt (2008), The THEMIS ESA plasma instrument and in-flight calibration, Space Sci. Rev., 141, 277-302, doi:10.1007/s11214-008-9440-2.

Min, K., K. Liu, and W. Li (2014), Signatures of electron Landau resonant interactions with chorus waves from THEMIS observations, J. Geophys. Res. Space Physics, 119, 5551-5560, doi:10.1002/2014JA019903.

Ni, B., Zou, Z., Li, X., Bortnik, J., Xie, L., & Gu, X. (2016). Occurrence characteristics of outer zone relativistic electron butterfly distribution: A survey of Van Allen Probes REPT measurements. Geophysical Research Letters, 43, 5644-5652. https://doi.org/10.1002/2016GL069350

Nowada, M., J.-H. Shue, C.-H. Lin, T. Sakurai, D. G. Sibeck, V. Angelopoulos, C. W. Carlson, and H.-U. Auster (2009), Alfve´nic plasma velocity variations observed at the inner edge of the low-latitude boundary layer induced by the magnetosheath mirror mode waves: A THEMIS observation, J. Geophys. Res., 114, A07208, doi:10.1029/2008JA014033.

Omura, Y., and D. Summers (2004), Computer simulations of relativistic whistler-mode wave-particle interactions, Phys. Plasmas, 11, 3530, doi:10.1063/1.1757457.

Rae, I. J., I. R. Mann, C. E. Watt, L. M. Kistler, and W. Baumjohann (2007), Equator-S observations of drift mirror mode waves in the dawnside magnetosphere, J. Geophys. Res., 112(A11), A11203, doi:10.1029/2006JA012064.

Roederer, J. G. (1967), On the adiabatic motion of energetic particles in a model magnetosphere, J. Geophys. Res., 72(3), 981-992, doi:10.1029/JZ072i003p00981.

Roux, A., O. Le Contel, C. Coillot, A. Bouabdellah, B. de la Porte, D. Alison, S. Ruocco, and M. C. Vassal (2008), The search coil magnetometer for THEMIS, Space Sci. Rev., 141, 265-275, doi:10.1007/s11214-008-9455-8.

Russell, C. T., Riedler, W., Schwingenshuh, K., & Yeroshenko, Y. (1987). Mirror instability in the magnetosphere of comet Halley. Geophysical Research Letters, 14, 644.

Shi, Q. Q., Pu, Z. Y., Soucek, J., Zong, Q. G., Fu, S. Y., Xie, L., et al. (2009). Spatial structures of magnetic depression in the Earth's high-altitude cusp: Cluster multipoint observations. Journal of Geophysical Research, 114, A10202. https://doi.org/10.1029/2009JA014283

Sibeck, D. G., R. W. McEntire, A. T. Y. Lui, R. E. Lopez, and S. M. Krimigis (1987), Magnetic field drift shell splitting: Cause of unusual dayside particle pitch angle distributions during storms and substorms, J. Geophys. Res., 92(A12), 13,485-13,497, doi:10.1029/JA092ia12p13485.

Soucek, J., & Escoubet, C. P. (2011). Cluster observations of trapped ions interacting with magnetosheath mirror modes. Annales Geophysicae, 29(6), 1049–1060. https://doi.org/10.5194/angeo- 29- 1049- 2011

Southwood, D. J., & Kivelson, M. G. (1993). Mirror instability. I—Physical mechanism of linear instability. Journal of Geophysical Research, 98, 9181– 9187. https://doi.org/10.1029/92JA02837

Sun, W. J., Shi, Q. Q., Fu, S. Y., Pu, Z. Y., Dunlop, M. W., Walsh, A. P., et al. (2012). Cluster and TC-1 observation of magnetic holes in the plasma sheet. Annales de Geophysique, 30(3), 583-595. https://doi.org/10.5194/angeo-30-583-2012

Takahashi K, Higbie P R, Baker D N. (1985) Azimuthal propagation and frequency characteristic of compressional Pc5 waves observed at geostationary orbit. J Geophys Res, 1985, 90: 1473–1485

Takahashi, K., L. J. Zanetti, T. A. Potemra, and M. H. Acuña (1987a), A model for the harmonic of compressional Pc5 waves, Geophys. Res. Let., 14, 363–366.

Takahashi, K., R. E. Lopez, R. W. McEntire, L. J. Zanetti, L. M. Kistler, and F. M. Ipavich (1987b), An easward propagating compressional Pc5 wave observed by AMPTE/CCE in the postmidnight sector, J. Geophys. Res., 92, 13,472–13,484.

Takahashi, K., C. Z. Cheng, R. W. McEntire, and L. M. Kistler (1990), Observation and theory of Pc5 waves with harmonically related transverse and compressional components, J. Geophys. Res., 95, 977–989.

Tian A M, Zong Q G, Shi Q Q. (2012) Reconstruction of morningside plasma sheet compressional ULF Pc5 wave. Sci China Tech Sci, 55: 1092–1100

Tian, A. M., Xiao, K., Degeling, A. W., Shi, Q. Q., et al. (2020). Reconstruction of plasma structure with anisotropic pressure: Application to Pc5 compressional wave. The Astrophysical Journal, 889, 35. https://doi.org/10.3847/1538-4357/ab6296

Thorne, R. M., & Tsurutani, B. T. (1981). The generation mechanism for magnetosheath lion roars. Nature, 293(5831), 384–386. https://doi.org/10.1038/293384a0

Thorne, R. M., B. Ni, X. Tao, R. B. Horne, and N. P. Meredith (2010), Scattering by chorus waves as the dominant cause of diffuse auroral precipitation, Nature, 467, 943–946, doi:10.1038/nature09467.

Tsurutani, B. T., and E. J.Smith (1974), Postmidnight chorus: Asubstormphenomenon, J. Geophys. Res., 79, 118–127, doi:10.1029/JA079i001p00118.

Wang, G. Q., Zhang, T. L., Xiao, S. D., Wu, M. Y., Wang, G., Liu, L. J., et al. (2020). Statistical properties of sub- ion magnetic holes in the solar wind at 1 AU. Journal of Geophysical Research: Space Physics, 125, e2020JA028320. https://doi.org/10.1029/2020JA028320

West, H. I., Jr., R. M. Buck, and J. R. Walton (1973), Electron pitch angle distributions throughout the magnetosphere as observed on Ogo 5, J. Geophys. Res., 78, 1064–1081, doi:10.1029/JA078i007p01064.

Xia, Z., Chen, L., Dai, L., Claudepierre, S. G., Chan, A. A., Soto- Chavez, A. R., & Reeves, G. D. (2016). Modulation of chorus intensity by ULF waves deep in the inner magnetosphere. Geophysical Research Letters, 43, 9444–9452. https://doi.org/10.1002/2016GL070280

Xiao, T., Shi, Q. Q., Tian, A. M., Sun, W. J., Zhang, H., Shen, X. C., & Du, A. M. (2014). Plasma and magnetic-field characteristics of magnetic decreases in the solar wind at 1 AU: Cluster-C1 observations. Solar Physics, 289(8), 3175-3195. https://doi.org/10.1007/s11207-014-0521-y

Xiao, T., Shi, Q. Q., Zhang, T. L., Fu, S. Y., Li, L., Zong, Q. G., et al. (2010). Cluster-C1 observations on the geometrical structure of linear magnetic holes in the solar wind at 1 AU. Annales de Geophysique, 28(9), 1695-1702. https://doi.org/10.5194/angeo-28-1695-2010

Yao, S. T., Wang, X. G., Shi, Q. Q., Pitkänen, T., Hamrin, M., Yao, Z. H., Li, Z. Y., Ji, X. F., De Spiegeleer, A., … Liu, J. (2017). Observations of kinetic-size magnetic holes in the magnetosheath. J. Geophys. Res., 122(2), 1999–2000. https://doi.org/10.1002/2016JA023858

Yao, S. T., Shi, Q. Q., Liu, J., Yao, Z. H., Guo, R. L., Ahmadi, N., et al. (2018). Electron dynamics in magnetosheath mirror mode structures. Journal of Geophysical Research: Space Physics, 123, 5561–5570. https://doi.org/10.1029/2018JA025607

Yao, S. T., Shi, Q. Q., Yao, Z. H., Li, J. X., Yue, C., Tao, X., et al. (2019a). Waves in kinetic-scale magnetic dips: MMS observations in the magnetosheath. Geophysical Research Letters, 46, 523–533. https://doi.org/10.1029/2018GL080696

Yao, S. T., Shi, Q. Q., Yao, Z. H., Guo, R. L., Zong, Q.-G., Wang, X. G., Degeling, A. W., Rae, I. J., Russell, C. T., and Tian, A. M. (2019b). Electron mirror-mode structure: magnetospheric

multiscale observations. Astrophys. J. Lett., 881(2), L31. https://doi.org/10.3847/2041-8213/ab3398

Yao, S. T., Hamrin, M., Shi, Q. Q., Yao, Z. H., Degeling, A. W., Zong, Q.-G., Liu, H., Tian, A. M., Liu, J., … Giles, B. L. (2020). Propagating and dynamic properties of magnetic dips in the dayside magnetosheath: MMS observations. J. Geophys. Res., 124(6), e2019JA026736. https://doi.org/10.1029/2019JA026736

Zhang, T. L., Russell, C. T., Baumjohann, W., Jian, L. K., Balikhin, M. A., Cao, J. B., et al. (2008). Characteristic size and shape of the mirror mode structures in the solar wind at 0.72 AU. Geophysical Research Letters, 35, L10106. https://doi.org/10.1029/2008GL033793

Zhang, X. J., Chen, L., Artemyev, A. V., Angelopoulos, V., & Liu, X. (2019). Periodic excitation of chorus and ECH waves modulated by ultralow frequency compressions. Journal of Geophysical Research: Space Physics, 124, 8535–8550. https://doi.org/10.1029/2019JA027201

Zhou, X. Z., Wang, Z. H., Zong, Q. G., Claudepierre, S. G., Mann, I. R., Kivelson, M. G., & Pu, Z. Y. (2015). Imprints of impulse-excited hydromagnetic waves on electrons in the Van Allen radiation belts. Geophysical Research Letters, 42, 6199–6204. https://doi.org/10.1002/2015GL064988

Zhou, X. Z., Wang, Z. H., Zong, Q. G., Rankin, R., Kivelson, M. G., Chen, X. R., & Kletzing, C. A. (2016). Charged particle behavior in the growth and damping stages of ultralow frequency waves: Theory and Van Allen Probes observations. Journal of Geophysical Research: Space Physics, 121, 3254–3263. https://doi.org/10.1002/2016JA022447

Zhu, X., and M. G. Kivelson (1991), Compressional ULF waves in the outer magnetosphere: 1. Statistical study, J. Geophys. Res., 96, 19,451–19,467.

Zhu, X., and M. G. Kivelson (1994), Compressional ULF waves in the outer magnetosphere: 2.

A case study of Pc5 type wave activity, J. Geophys. Res., 99, 241–252, doi:10.1029/93JA02106.

Zong Q G, Zhou X Z, Li X, et al. (2007) Ultralow frequency modulation of energetic particles in the dayside magnetosphere. Geophys Res Lett, 34: L12105

Zong Q G, Zhou X Z, Wang Y F, et al. (2009) Energetic electron response to ULF waves induced by interplanetary shocks in the outer radiation belt. J Geophys Res, 114: A10204

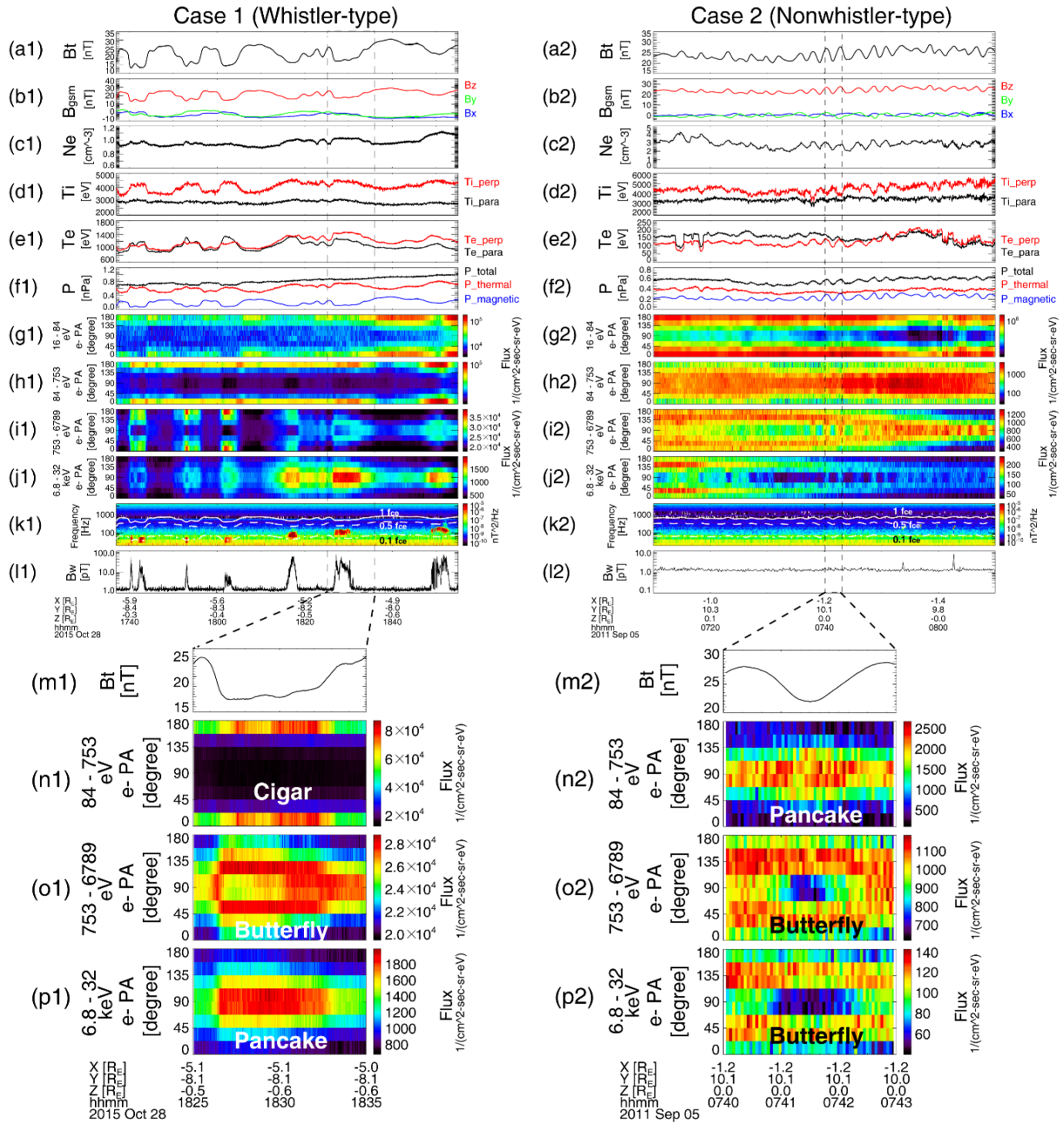

Figure1. Overview of the two compressional Pc5 wave cases. Left (Case 1, THEMIS A 17:32–18:55 UT on October 10, 2015) and right (Case 2, THEMIS A 07:10–08:10 UT on September 5, 2011) columns represent whistler-type and nonwhistler-type cases, respectively. For both of two cases: (a) Total magnetic field; (b) components of the magnetic field in geocentric solar magnetospheric (GSM) coordinates; (c) electron number density; (d) ion temperature in perpendicular (red) and parallel (black) directions; (e) electron temperature in perpendicular (red) and parallel (black) directions; (f) total pressure (black), plasma thermal pressure (red) and

magnetic pressure (blue); (g)–(j) ePADs of four energy ranges: 10–84 eV, 84–753 eV, 753 eV–6.8 keV and 6.8–32 keV, respectively; (k) Time-frequency spectrogram of the wave magnetic fields (solid, dashed and dot-dashed lines represent f_{ce}, 0.5 f_{ce} and 0.1 f_{ce}, respectively) from the DFB; (l) integrated whistler wave amplitude over 0.05 f_{ce}–0.5 f_{ce}; (m, n, o, and p) are the same as (a, h, i, and j) at time ranges of the magnetic troughs (dashed rectangles).

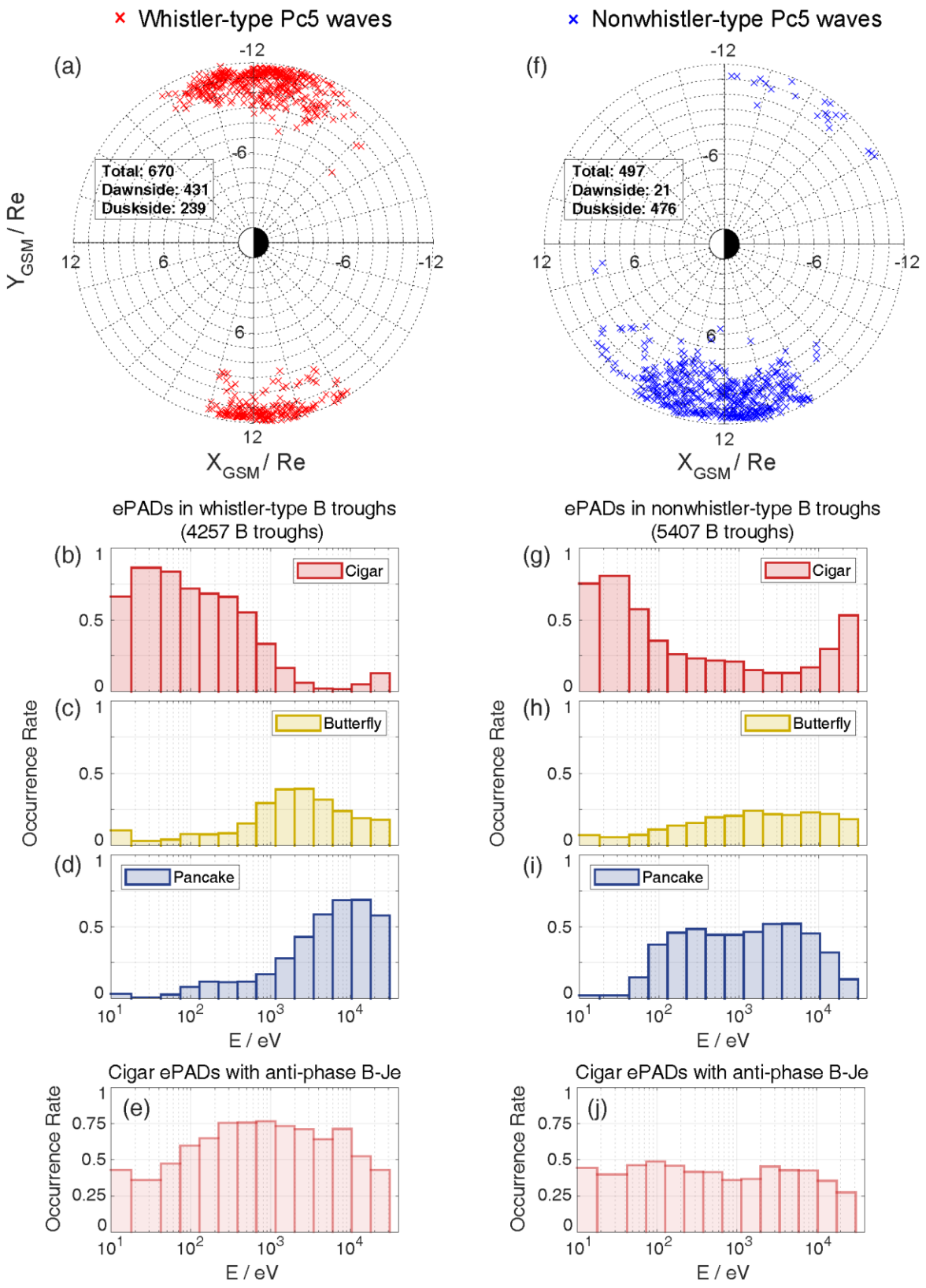

Figure 2. Global distributions of (a) whistler-type compressional waves, (f) nonwhistler-type compressional waves and the occurrence rate for cigar, butterfly, pancake ePADs and cigar ePAD with anti-phase B-Je oscillations in the whistler-type (b–e) and nonwhistler-type (g–j) magnetic troughs.

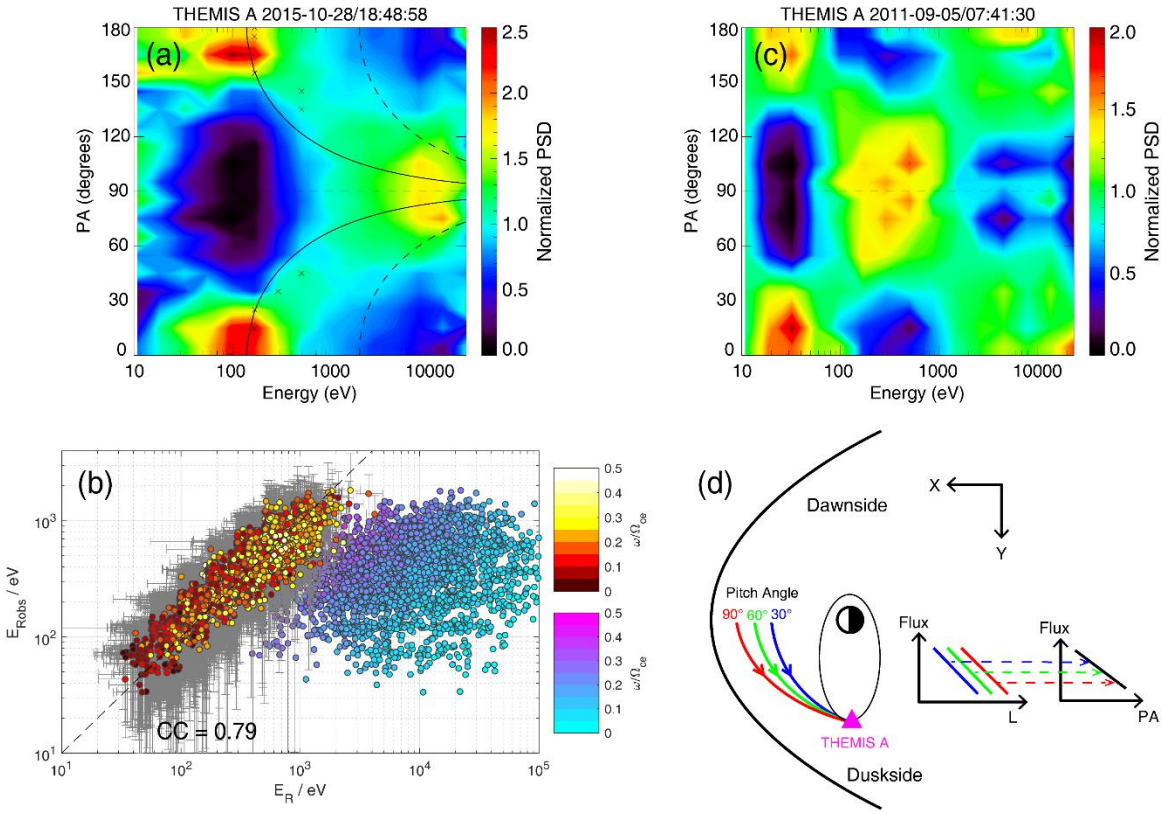

Figure 3. (a) Electron pitch angle-energy spectrogram at 18:48:58 UT on October 28, 2015 in case 1. Solid and dashed curves represent Landau and cyclotron resonant energies. Crosses represent the points to calculate the parallel energies of the electrons with the maximum PSDs within 0–60° and 120°–180° pitch angle bins. (b) Correlation of the resonant energies (hot color dots: Landau resonance, cool color dots: cyclotron resonance) and E_{Robs}. Black dashed line represents that the Landau resonant energies are equal to the E_{Robs}. Vertical error bars represent one standard deviations of E_{fmax}*cos^2(PA_{fmax}) and horizontal error bars represent the errors from the WNA uncertainty. (c) Electron pitch angle-energy spectrogram at 2011-09-05/07:41:30 (UT) in case 2. (d) Diagram of the drift-shell splitting effect of the electrons.